Journal of Materials Chemistry B

Materials for biology and medicine

rsc.li/materials-b

ROYAL SOCIETY OF CHEMISTRY
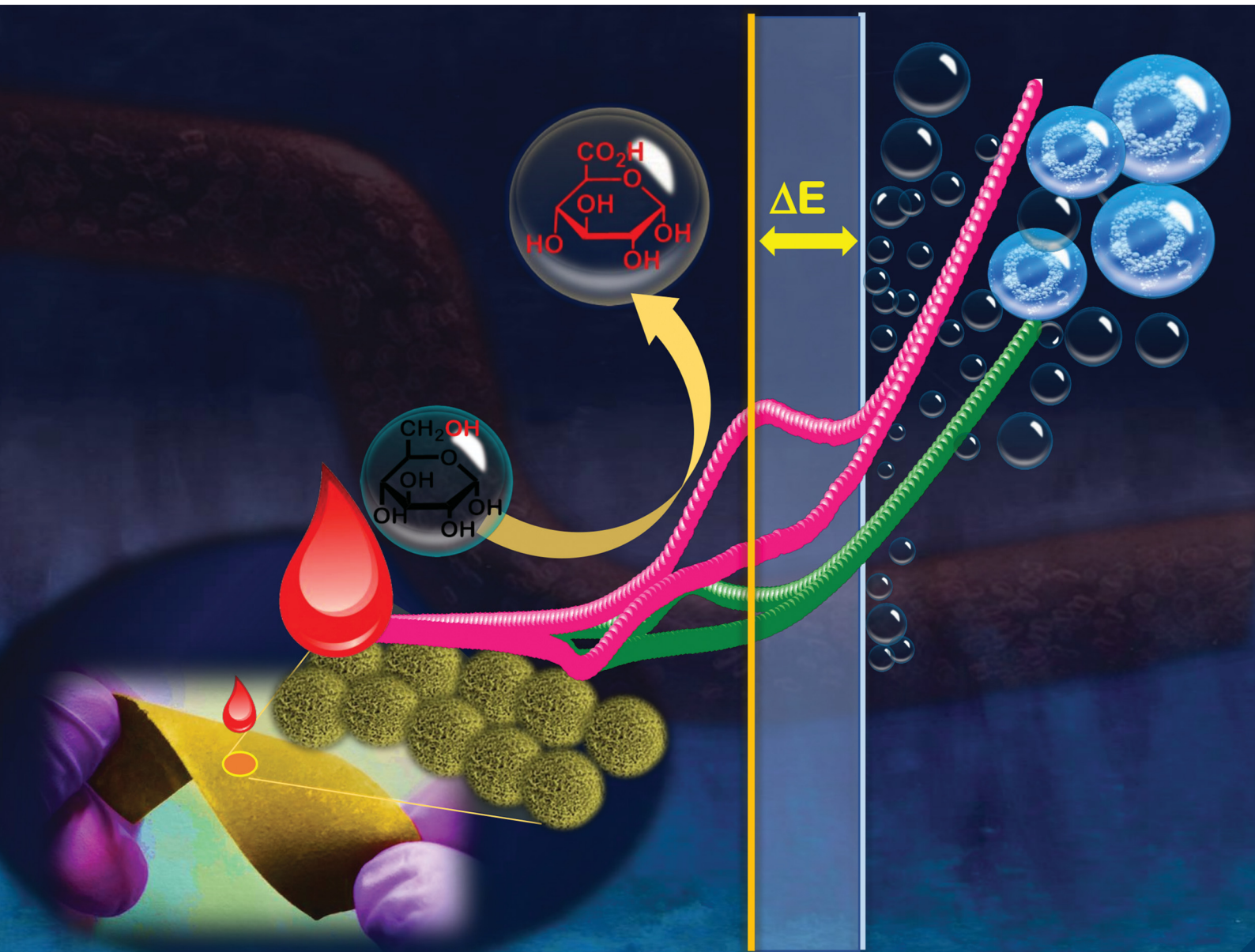
PAPER
Debaprasad Mandal, Tharamani C. Nagaiah *et al.*
Highly sensitive non-enzymatic electrochemical glucose
sensor surpassing water oxidation interference

Indexed in Medline!

PAPER

Check for updates

Highly sensitive non-enzymatic electrochemical glucose sensor surpassing water oxidation interference†

Neha Thakur, Debaprasad Mandal [ID] * and Tharamani C. Nagaiah [ID] *

An electrochemical non-enzymatic sensor based on a NiVP/Pi material was developed for the selective and sensitive determination of glucose. The novel sensor showed a high sensitivity of 6.04 mA μM^{-1} cm^{-2} with a lowest detection limit of 3.7 nM in a wide detection range of 100 nM–10 mM. The proposed sensor exhibited a superior selectivity without any interference from the oxygen evolution reaction during glucose sensing. We also found that this glucose sensor showed negligible interference from various interferents, such as ascorbic acid, uric acid, dopamine and sodium chloride. Additionally, a novel flexible sensor was developed by coating the NiVP/Pi over Whatman filter paper, which exhibited two linear ranges of 100 nM to 1 μM and 100 μM to 10 mM with an ultra-sensitivity of 1.130 mA μM^{-1} cm^{-2} and 0.746 mA μM^{-1} cm^{-2}, respectively, in 0.1 M NaOH. The proposed sensor was tested with human blood serum samples demonstrating its practical application. Our findings provide a new route by fine tuning the composition of nickel and vanadium that sheds new light on better understanding the processes. This NiVP/Pi-based sensor offers a new approach towards the electrochemical detection of glucose, enabling glucose monitoring in a convenient way.

1. Introduction

Globally, coronavirus disease 2019 (COVID-19), which spreads through Severe Acute Respiratory Syndrome Coronavirus 2 (SARS-Cov-2), has triggered extensive damage to public health globally and is continuing to spread rapidly.[1–3] Recent studies have shown the connection between blood glucose levels and the clinical course of SARS.[4] People with diabetes developing COVID-19 are at increased risk of its complications leading to increased morbidity and mortality rates. Diabetes has been recognized as a menace factor for COVID-19.[5]

Diabetes mellitus is a worldwide human health problem caused mainly by the deficiency of insulin, which is measured by an abnormal level of blood glucose concentration.[6,7] Glucose is a vital biomolecule of the human body and the normal range lies in the range of 80–120 mg dL^{-1} (4.4–6.6 mM) for a healthy person.[8] However, any deviation can cause several disorders, including blindness, heart attack, nerve damage and kidney failure.[6] Consequently, glucose sensors have been receiving widespread attention as 85% of the entire biosensor markets are covered by it.[9] Moreover, the measurement of the glucose concentration has attracted considerable attention in other fields,

such as in the food industry and environmental protection field along with clinical diagnostics.[10,11] Among the various techniques used for the detection of fluctuating levels of glucose in the body, electrochemical methods are in vogue due to their low cost, rapid response, high sensitivity, point-of-care detection capability and more importantly, easy electro-oxidation of glucose, which makes it a more viable technique.[12,13] In the past decade, enzyme-based electrochemical sensors have been reported extensively and the commercially available disposable glucose biosensor is an enzyme-based system, which in general relies on the immobilization of glucose oxidase (GO_x)/glucose dehydrogenase (GDH) enzyme on to a suitable matrix.[14–16] However, major drawbacks associated with these enzyme based sensors are the denaturation of the expensive enzyme, poor reproducibility and complex immobilization procedure.[6,17] Considering the rapid growth of world population with increased number of diabetic persons at $\sim$422 million in 2020 and expected to be 642 million by 2030 as per the World Health Organization (WHO) and International Diabetes Federations (IDF),[18] the development of a highly sensitive with accurate and cost-effective sensor is of great demand.

Alternatively, the non-enzymatic electro-oxidation of glucose has been explored extensively using various noble metals to non-noble metals, including Zn, Cu, Co, Ni, Mn and Fe, and Cu along with metal oxides and sulfides.[11,19–24] Although, these successful efforts eliminate the requirement for expensive enzymes, interference from the oxygen evolution reaction (OER),[25] which is the

Department of Chemistry, Indian Institute of Technology Ropar, Rupnagar, Punjab, 140001, India. E-mail: dmandal@iitrpr.ac.in, tharamani@iitrpr.ac.in
† Electronic supplementary information (ESI) available. See DOI: 10.1039/d1tb01332g

This journal is © The Royal Society of Chemistry 2021

J. Mater. Chem. B, 2021, **9**, 8399–8405 | 8399

anodic half-reaction of the overall electrochemical water splitting reaction, makes the sensor unreliable since the onset potential for OER is close to that of the glucose oxidation potential. More importantly, O_2 gas bubbles arising during OER can cover the active sites and thus weaken the oxidation ability for glucose.[21] So, the most appropriate approach to eliminate the interference is achieved by ensuring a large potential difference between the onset potential for OER and the glucose oxidation potential. In this context, not much attention has been given to this issue yet and so far only one recent report is available wherein an NiFe-LDH material for glucose sensing was shown to be able to differentiate the glucose oxidation reaction from the OER through its minimum interference.[21] However, LDHs suffer from a poor electronic conductivity, which ultimately hinders their practical application. Subsequently, transition metal phosphide/phosphates (TMP/Pi) are gaining increasing interest in electrocatalytic applications due to their high conductivity and stability, and better corrosion resistivity.[26–28]

Herein, we explored nickel vanadium phosphide/phosphate (NiVP/Pi) as an efficient catalyst for the selective oxidation of glucose. The proposed non-enzymatic sensor was also tested for the quantitative estimation of glucose in human blood serum samples at physiological pH, showing good agreement with the data measured in the hospital. Further, we demonstrated a flexible paper electrode with our proposed catalyst NiVP/Pi as a promising sensor that could be used an everyday tool in wearable bioelectronic technology for the direct electrochemical sensing of glucose. Flexible electronics have attracted widespread attention due to their potential for future hand-held, portable consumer and wearable electronics.[29] The integration of these sensor systems in smartphones and other wearable electronic devices enhances the management of diabetes by significantly increasing the widespread accessibility of glucose monitoring platforms.

2. Experimental section

2.1. Materials and reagents

All chemicals were used without further purification. $NiCl_2 \cdot 6H_2O$ (97%), ammonium metavanadate (99%), red phosphorus (98%, crystalline), ammonium fluoride (98%, crystalline), potassium hydroxide pellets and sodium chloride were acquired from Loba Chemie. Glucose (>99%,), dopamine hydrochloride (>99% crystalline), ascorbic acid (99%) and uric acid were from Sigma-Aldrich. Sodium hydroxide was procured from Alfa Aesar. Potassium dihydrogen phosphate (KH_2PO_4), dipotassium hydrogen phosphate (K_2HPO_4), urea and isopropanol were procured from Merck. Deionized water was obtained from a Millipore system (>12 MΩ cm^{-1}). PBS (0.1 M) was prepared from stock solutions of 0.1 M KH_2PO_4 and 0.1 M K_2HPO_4.

2.2. Synthesis of NiVP/Pi

Initially, the precursor was prepared by hydrothermal treatment followed by a low-temperature microwave-assisted phosphidation reaction. In the first step, a mixture of a 1:1 molar ratio of $NiCl_2 \cdot 6H_2O$ and NH_4VO_3 was added in to 35 mL of water under

stirring for 10 min to form a homogeneous solution. Next, 18 mmol of urea and ammonium fluoride was added to the reaction mixture, and stirred for 30 min till a homogeneous solution was obtained. The solution was transferred into a 50 mL Teflon-lined autoclave and heated at 120 °C for 6 h. After cooling, the resulting brown suspension (precipitate) of $NiV(OH)_2$ was filtered and washed with a (1:1) water and ethanol mixture (3 × 10 mL) and dried overnight at 60 °C.

Second step. The obtained brown nickel vanadium layer double hydroxides (0.300 g) was mixed with 0.100 g of red phosphorous suspended in 10 mL water and transferred to a microwave vial and purged with N_2 gas for 10 min. The sample was irradiated in a Multiwave Pro instrument (Anton Paar) at 100 °C with a 15 min ramp and holding for 30 min at 100 °C, under a limiting pressure of 18 bar at 600 Watt by a controlled temperature programme. The obtained precipitate was filtered and washed (3 × 30 mL) with deionized water and dried at 60 °C in an oven. Other variants of NiVP/Pi were also synthesized similarly, by varying the ratio of $NiCl_2 \cdot 6H_2O$, NH_4VO_3 (different Ni:V molar ratios) (detailed in Table S1, ESI†).

Similarly, NiP/Pi and VP/Pi were synthesized under similar reaction conditions as above using only $NiCl_2 \cdot 6H_2O$ and NH_4VO_3, respectively.

2.3. Physical characterization

NiVP/Pi was characterized using X-ray powder diffraction (XRD) in the range of 10°–80° at a scan speed of 2° per min on a PANalytical X'PERT pro diffractometer using Cu Kα radiation (λ = 0.1542 nm, 40 kV, 40 mA). The morphology of the catalyst was performed by scanning microscopy (SEM; JEOL, JSM-6610 LV). Further, the in-depth morphology and elemental distribution were recorded by high-resolution transmission electron microscopy (HR-TEM) and scanning transmission electron microscopy (STEM) using a FEI Tecnai instrument (G2 F20, Netherlands), operating at 200 keV. The surface elemental composition and in-depth analysis of the functional groups were carried out using X-ray photoelectron spectroscopy (XPS) on a Thermo Scientific NEXSA surface analysis system (working at 72 W, 12 000 V) under an ultrahigh vacuum (UHV 8–10 mbar). The X-ray source used for the sample analysis was monochromatic Al Kα radiation (1486.6 eV). The spectra were standardized with respect to the C (1s) peak at 284.5 eV with a precision of ±0.2 eV.

2.4. Electrochemical measurements

All the electrochemical experiments were carried out using a three-electrode assembly in a single compartment electrochemical workstation, (Bio-Logic (VSP 300)) consisting of catalyst-modified Ni foam (thickness: 1.6 mm, 0.12 cm^2) as the working electrode (WE), Ag/AgCl/3 M KCl double junction as the reference electrode (RE) and Pt wire as the counter electrode (CE), for glucose sensing, and 0.1 M NaOH was used as the electrolyte.

The NiVP/Pi catalyst slurry was prepared by dispersing 1.25 mg of the catalyst in 500 μL of a solution containing isopropyl alcohol (IPA, 100 μL), and Millipore water (400 μL, 12 MΩ), by ultrasonication for 30 min. Afterwards, 40 μL (100 μg) of the as-prepared homogeneous slurry was drop-cast on the Ni

8400 | *J. Mater. Chem. B*, 2021, **9**, 8399–8405

This journal is © The Royal Society of Chemistry 2021

foam and dried at room temperature. Before use, the Ni foam was cleaned with 1 M HCl solution and washed with ethanol and distilled water, respectively. Electrochemical impedance measurements (EIS) were conducted at a DC voltage of 0.54 V over a frequency range between 20 mHz to 3 MHz. Each experiment was repeated at least 5–6 times to ensure the reproducibility.

3. Result and discussion

The NiVP/Pi with different metal ratios were synthesized from the corresponding NiV layered double hydroxide (NiV-LDH) by a low-temperature phosphidation reaction under microwave irradiation using red phosphorous without disrupting the NiV-LDH lattice, since lattice disruption would lead to poor activity[30] (synthesis details are provided in the ESI†).

Nevertheless, the catalytic activity of these materials strongly depends on their composition. Consequently, the present study focused on adjusting the stoichiometry of nickel and vanadium, which was confirmed by microwave plasma atomic emission spectrometry (MP-AES) (Table S2, ESI†). The morphology and oxidation state of the synthesized materials were analysed by scanning electron microscopy (SEM), transmission electron microscopy (TEM) and X-ray photoelectron spectroscopy (XPS). The SEM images of NiV(2:1)P/Pi depicted in Fig. 1b (Fig. S1, ESI†) exhibit closely packed microspheres morphology resulting from the multilayers of crosslinked numerous ultrathin nanosheets that are almost perpendicular to the surface, forming a 3D network structure of spheres. These nanosheets were further confirmed by TEM and high-resolution TEM (Fig. 1c). The selected area electron diffraction (SAED) pattern in Fig. 1c (inset) shows the lower crystallinity due to the nanosheet structure. Further the HRTEM image (Fig. 1c, inset) displays lattice fringes with a lattice spacing of 0.702, 0.254 and 0.28 nm, corresponding to the (010) plane of $NiPO_4$, (012) of NiV-LDH and (051) plane of NiP, respectively. Subsequently, scanning transmission electron microscopy (STEM) line spectra were collected for NiV(2:1)P/Pi (Fig. S2, ESI†), which confirmed the coexistence of all the elements Ni, V, P and O, which were uniformly distributed in the scanned area (blue line).

The XPS survey spectra further supported the presence of all the elements Ni, Fe and P along with O with no impurities (Fig. 1d). The Ni 2p spectrum of NiV(2:1)P/Pi could be deconvoluted into two peaks centred at 873.3 and 855.6 eV, corresponding to Ni $2p_{1/2}$ and Ni $2p_{3/2}$, respectively, along with satellite peaks at 879.4 and 861.1 eV due to the oxidized Ni species (Ni^{2+} species).[31] Similarly, the deconvoluted V 2p XP spectrum revealed V $2p_{1/2}$ and V $2p_{3/2}$ peaks due to spin–orbit coupling and the peak of V $2p_{3/2}$ could be fitted into two constituent peaks corresponding to V^{4+} (516.7 eV) and V^{5+} (517.5 eV). The P 2p spectrum showed a phosphate peak at higher binding energy (133.4 eV) and phosphide peak at 129.8 eV. Also, the XP O 2p spectra displayed two peaks, located at 530.3 and 531.3 eV, which could be assigned to O^{2-} and OH^{-}, respectively (Fig. 1e–g and Fig. S3, ESI†). The microstructural attributes of the synthesized materials were analysed by powder X-ray diffraction (XRD). The diffraction peaks and SEM of the NiV-LDH precursor well matched with those of NiVP/Pi (Fig. S1 and S3, ESI†). The XRD patterns (Fig. S3, ESI†) demonstrated that the NiVP/Pi catalysts were composed of $NiPO_4$ (ICSD ID-74049) and NiP (ICSD ID-188064) NiV-LDH[32,33] mixed phases, thereby confirming the successful formation of nickel vanadium phosphide/phosphate, which was consistent with the HRTEM results.

To study the applicability of the novel NiVP/Pi catalyst towards the electrochemical oxidation of glucose, initially cyclic voltammetric (CV) measurements were performed using different variants of NiVP/Pi catalyst coated on a Ni foam in 0.1 M NaOH without any analyte. A well-defined redox behaviour corresponding to the oxidation of Ni(II) to Ni(III) was found, which upon variation of the metal ratio, it was found that the oxidation peak potential (E_{ox}) varied as $ca.$ 1.43, 1.36, 1.39 and 1.44 V for NiV(1:2), NiV(1:1), NiV(2:1) and NiV(3:1)P/Pi, respectively (Fig. 2a and Fig. S4, ESI†).
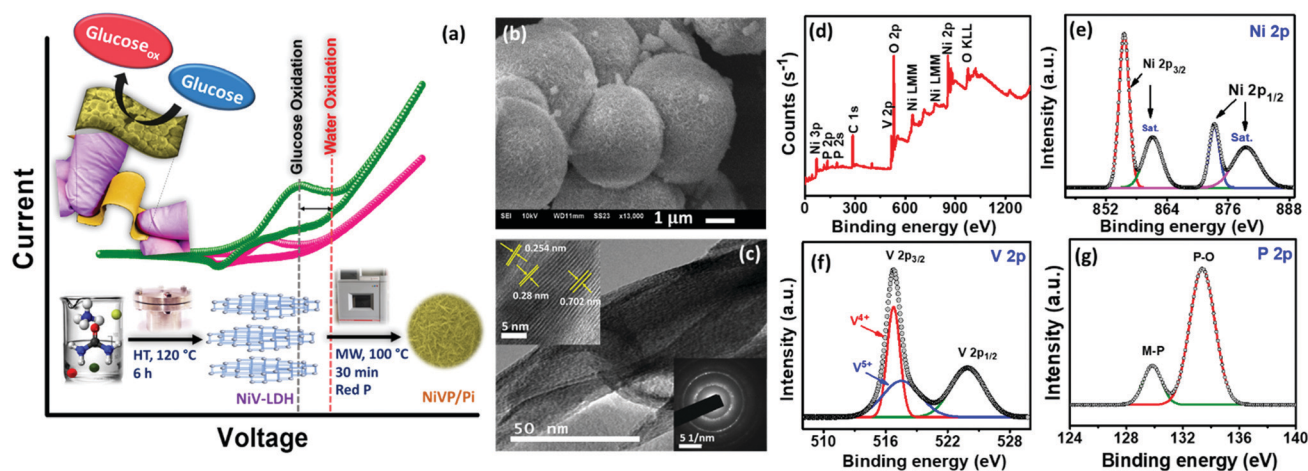

Fig. 1 (a) Schematic representation of the preparation process and glucose detection with the NiVP/Pi catalyst; (b) SEM and (c) TEM images (inset: SAED pattern, HRTEM image) of NiV(2:1)P/Pi catalyst; (d) XP survey spectra and deconvoluted XP spectra of the: (e) Ni 2p, (f) V 2p and (g) P 2p of NiV(2:1)P/Pi catalyst.
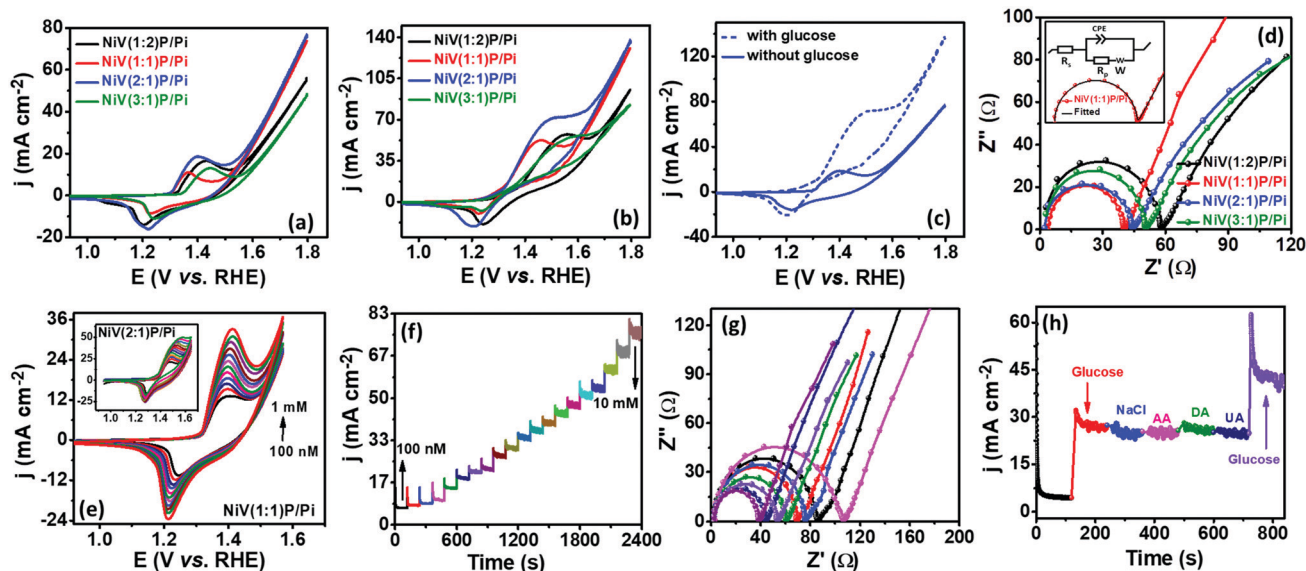
Fig. 2 CV of various NiVP/Pi (a) without and (b) with 10 mM of glucose, and (c) comparison of NiV(2 : 1)P/Pi in 0.1 M NaOH electrolyte at a scan rate of 5 mV s^{-1}, (d) corresponding EIS studies (inset: fitted equivalent circuit of NiV(1 : 1)P/Pi); (e) CV (inset: CV of NiV(2 : 1)P/Pi), (f) chronoamperometric, and (g) EIS response of NiV(1 : 1)P/Pi on Ni foam in 0.1 M NaOH electrolyte at various conc. of glucose, EIS at frequency ranging from 20 mHz to 3 MHz, (h) chronoamperometric response curve of NiV(1 : 1)P/Pi after the successive addition of 1 mM glucose, 1 mM NaCl, 1 mM AA, 1 mM DA, 1 mM UA and 1 mM glucose in 0.1 M NaOH solution, CE: Pt wire, RE: double junction Ag/AgCl/3 M KCl.

It was observed that after the oxidation potential, there was a sharp increase in the current for all the variants, which could be attributed to the OER. Interestingly, changes in the CV behaviour were observed upon the addition of 10 mM glucose with a rapid increase in the current, indicating a good catalytic activity towards the electro-oxidation of glucose (Fig. 2b) wherein Ni(II) was electrochemically oxidized to Ni(O)OH [Ni(III)] in NaOH and subsequently, glucose was oxidized to gluconolactone/gluconic acid/glucaric acid (as confirmed by the HRMS studies, Fig. S5, ESI†) by Ni(III), which subsequently was reduced to Ni(II).[34] Interestingly, the cathodic peak current (Fig. 2b) was lower compared to the anodic peak current, which could be rationalized as follows: Ni(II) was oxidized to Ni(III), which was consumed in glucose oxidation, so the amount of Ni(III) left over was less; thus the lowering of reduction peak current demonstrated its efficacy in glucose oxidation.[35]

It is noteworthy to mention that the oxidation peak potential was shifted to more positive values, *ca.* 1.56, 1.46, 1.50 and 1.58 V for the NiV(1 : 2), NiV(1 : 1), NiV(2 : 1) and NiV(3 : 1)P/Pi, respectively, and the corresponding onset OER potentials were determined to be 1.64, 1.57, 1.62 and 1.67 V, respectively. So, to distinguish glucose oxidation with the OER, the difference between the OER onset potential and the glucose oxidation potential should be high and an electrocatalyst with a larger difference would thus be considered as ideal.[21] It was found that the potential differences for NiV(1 : 2), NiV(1 : 1), NiV(2 : 1) and NiV(3 : 1)P/Pi were calculated to be 0.08, 0.11, 0.12 and 0.09 V, respectively; thus both NiV(1 : 1) and NiV(2 : 1)P/Pi showed the least interference (Fig. 2c). This could be due to their better electron-transport properties at the electrode–electrolyte interface, as supported by the electrochemical impedance

spectroscopy (EIS) results. As observed from the Nyquist plot in Fig. 2d, the lowest R_{ct} was observed for NiV(1 : 1) and NiV(2 : 1) compared to the other variants. The lower R_{ct} signifies the dominance of the faster kinetics towards the electro-oxidation of glucose due to the facilitated electron transport at the catalyst surface.

To ascertain the applicability of the proposed catalyst as a sensor for glucose determination, the NiV(1 : 1)P/Pi variant was chosen due to its distinctive peak and then CV measurements were performed at various concentrations of glucose. As observed from the CV plot in Fig. 2e, the oxidation peak current increased with increase in glucose concentration from 100 nM to 1 mM, suggesting that the NiV(1 : 1)P/Pi catalyst can effectively catalyze glucose oxidation. Besides, the oxidation peak potential also shifted to more positive values, which can be attributed to the oxidation of adsorbed glucose molecules at higher potential as compared to the oxidation of Ni^{2+} species.[13] Moreover, the chronoamperometric measurement exhibited a step-like increase in the current density and remained constant after every 2 min of sequential glucose addition (100 nM–10 mM). The well-defined stepwise increased current further supported the electro-oxidation response of the catalyst towards the highly sensitive detection of glucose. For the sensitivity of the NiV(1 : 1)P/Pi catalyst, the calibration curve was obtained from chronoamperometry (Fig. 2f). It could be concluded that the calibration curve showed a good linear relationship between the current response and the concentration of glucose (Fig. S4c, ESI†). The linear response for the determination of glucose was found to be from 100 nM to 1 μM and 100 μM to 10 mM with a sensitivity of 6.04 mA μM^{-1} cm^{-2} and 4.46 mA μM^{-1} cm^{-2} respectively. Based on a signal-to-noise (S/N) ratio of 3, the limit of detection (LOD) was found to be 3.7 nM,

8402 | *J. Mater. Chem. B,* 2021, **9**, 8399–8405

This journal is © The Royal Society of Chemistry 2021

demonstrating an excellent electrochemical sensor performance. This was further supported by the EIS studies (Fig. 2g), wherein R_{ct} decreased with the increase in glucose concentration. It is noteworthy to mention that the semicircle decreased at a lower frequency with an increased concentration of glucose and no changes in the solution resistance was observed, signifying a faster kinetics towards the electro-oxidation of glucose. Further experiments with mono-metallic phosphide/phosphates catalysts (NiP/Pi and VP/Pi) and NiV-LDH exhibited a less intense peak compared to NiV(1:1)P/Pi (Fig. S6a, ESI†). It is clear that the addition of a second metal improved the sensor performance by efficiently manipulating the electronic properties of the material, leading to better electron-transport properties at the electrode–electrolyte interface, as supported by the EIS results. As observed from the Nyquist plot (Fig. S6b, ESI†) R_{ct} was higher for the mono-metallic phosphides/phosphates and nickel vanadium layer double hydroxides compared to the NiV(1:1)P/Pi catalyst; while NiV(1:1)P/Pi revealed the lowest R_{ct} compared to the other catalysts. A lower R_{ct} signifies the dominance of faster kinetics towards the electro-oxidation of glucose due to facilitated electron transport at the catalyst surface. This facile kinetics could be due to the available electrochemical active sites, which was calculated using the double layer capacitance in the non-faradaic region (Fig. S7, S8 and Table S3, detailed in ESI†). Thus the electrochemical surface area (ECSA) of the NiV(1:1)P/Pi catalyst was found to be 6.55 cm². The effect of the scan rate (10 to 100 mV s⁻¹) of the NiV(1:1)P/Pi material on the electrochemical response at 1 mM glucose was investigated by CV (Fig. S9, ESI†). The CV at various scan studies

revealed a linear relationship between the anodic peak current (I_{pa}) and the cathodic peak current (I_{pc}) vs. the square root of the scan rate, indicating that the electro-oxidation of glucose by NiV(1:1)P/Pi was a diffusion-controlled process (Fig. S9, ESI†).

The key challenge in designing a non-enzymatic electrochemical sensor is to selectively detect interfering agents present in real sample, such as uric acid (UA), dopamine (DA) and ascorbic acid (AA), as well as the inorganic salt NaCl. The chronoamperometric experiments at +0.54 V (Fig. 2h) showed an increased current response of the NiV(1:1)P/Pi catalyst upon the addition of 1 mM glucose and this remained constant. After injecting possible interfering reagents into the same electrolyte, the proposed sensor exhibited a negligible change in response. Additionally, an excellent stability for the NiV(1:1)P/Pi catalyst was also determined by recording its 100 consecutive CV curves (Fig. S10, ESI†). Moreover, we explored NiV(1:1)P/Pi as a flexible sensor by coating the catalyst on Whatman filter paper and using it as an electrode (details in the ESI†) for the direct electrochemical oxidation of glucose in 0.1 M NaOH. The proposed flexible sensor exhibited a wide detection range from 100 nM to 1 μM and 100 μM to 10 mM with an ultra-sensitivity of 1.130 mA μM⁻¹ cm⁻² and 0.746 mA μM⁻¹ cm⁻², respectively, in 0.1 M NaOH (Fig. 3a). We also performed the same experiments at physiological pH (0.1 M PBS) (Fig. 3b). The experiments were performed by applying a preconditioning potential of −2.0 V for 30 s on the NiV(1:1)P/Pi electrode followed by glucose addition for sensing. At this potential, protons were reduced on the electrode surface, which produced a localized alkaline environment on the
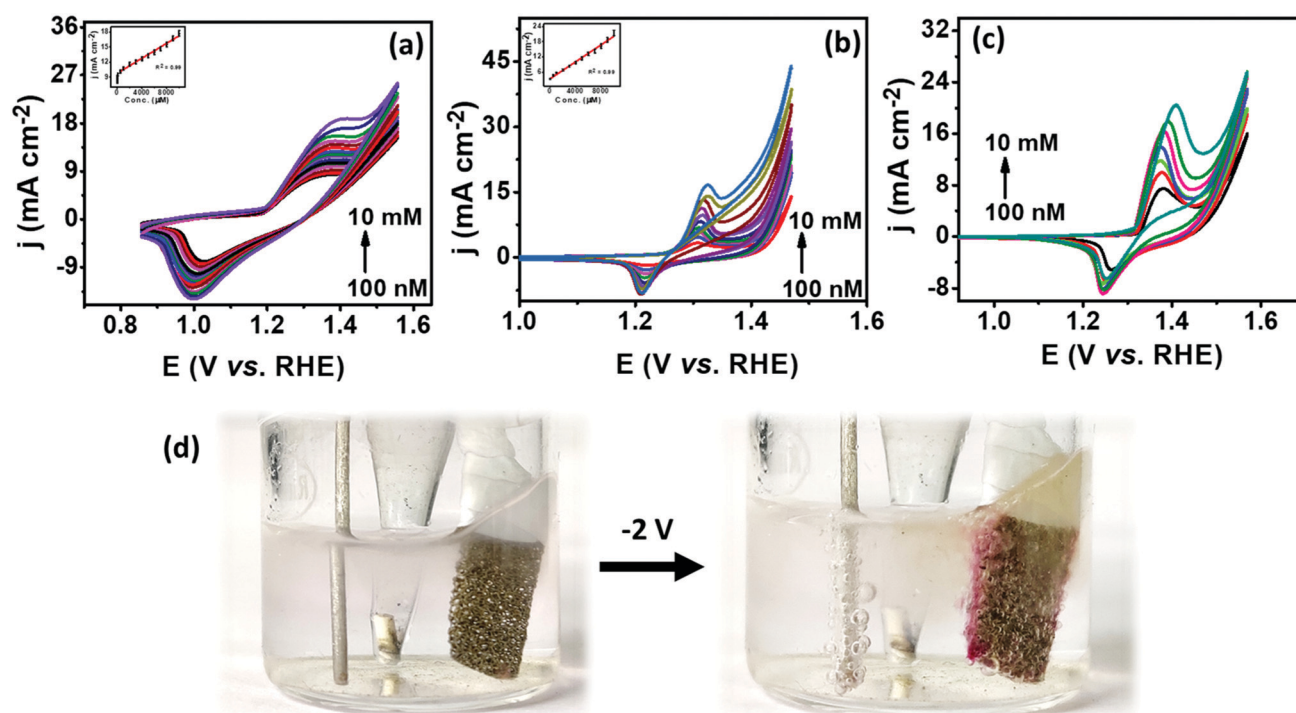

Fig. 3 CV response of NiV(1:1)P/Pi over the paper electrode in (a) 0.1 M NaOH electrolyte, (b) 0.1 M PBS electrolyte (pH 7.4) at various concentrations of glucose, (c) at various concentrations of glucose in blood serum samples, (d) images change of pH by applying −2 V in 0.1 M PBS solution containing 5 μL of 5% phenolphthalein (in ethanol) in the electrochemical cell, CE: Pt wire, RE: double junction Ag/AgCl/3 M KCl.

This journal is © The Royal Society of Chemistry 2021

J. Mater. Chem. B, 2021, 9, 8399–8405 | 8403

electrode surface for glucose detection.[36–38] The obtained cyclic voltammogram after preconditioning at −2.0 V exhibited a well-defined redox behaviour, corresponding to the Ni(II)/(III), as shown in the Fig. S11, ESI.† With the sequential addition of glucose, the peak currents increased (Fig. 3b), suggesting that the NiV(1 : 1)P/Pi catalyst could effectively catalyze electrochemical glucose oxidation even at physiological pH. The obtained oxidation current was found to be linearly correlated with the glucose concentration (inset) with a superior sensitivity of 1.67 mA μM^{-1} cm^{-2}, demonstrating its potential applications in portable devices which are cost-effective, eco-friendly, simple and disposable.

To ascertain the applicability of the proposed sensor in clinical diagnosis experiments, the proposed sensor was tested for the quantitative estimation of the glucose content in human blood serum samples in 0.1 M phosphate buffer (pH 7.4) at various glucose concentrations (Fig. 3c and Fig. S11, S12, ESI†). The local pH at the electrode/electrolyte interface was adjusted by applying a preconditioning potential (−2 V) on the NiVP/Pi electrode (Fig. 3c). At this potential, a localized alkaline environment on the electrode surface was observed for glucose detection.[36–38] Fig. 3d and Fig. S12A (ESI†) show the pH change at the electrode–electrolyte interface, as indicated by the pink colour of phenolphthalein during the pretreatment process, signifying the pH change from neutral to alkaline. After pretreatment, the pH near the working electrode gradually decreased due to diffusion, leading to neutralization with phosphate buffer, as shown by the colour change from pink back to colourless. Furthermore, after the pretreatment process, the pH change of the sample solution was observed by using a glass capillary near the working electrode and was tested using a pH test strip. Fig. S12B (ESI†) shows the colour change of the pH at different time intervals from 7.4 to about 13. Further measurements were done with a pH meter and it was found that the pH changed to ≈14 within 30 s and therefore it was chosen as ideal for comprehensive study, which would lead to an alkaline environment for activation of the catalyst for the non-enzymatic detection of glucose. To understand the nature of the proposed catalyst after the preconditioning process, a detailed investigation was performed by PXRD. Fig. S12C (ESI†) shows the peaks corresponding to NiV(1 : 1)P/Pi; however, the presence of a small fraction of metallic Ni/V could not be discarded since the peaks of metallic Ni (JCPDS card no. 03-065-2865) and metallic V (JCPDS card no. 00-022-1058) overlapped with NiVP/Pi.

The proposed sensor was tested with 25 μM glucose and the results were in a good agreement with the data measured in hospital. Further, recovery of the spiked sample (human serum blood) *via* a standard addition method exhibited ranges from 99–113% (Table S4, ESI†), demonstrating the efficacy of the proposed sensor for practical applications. Also, post analysis was carried out by XRD, XPS and EDX. The XPS spectra in Fig. 4 shows the presence of all the desired elements similar to the as-prepared catalyst. Remarkably, in the P 2p XP spectra, phosphide/phosphate species still remained, indicating the stability of the electrocatalyst. For the O 1s spectrum, the intensities of the oxides and hydroxides increased after glucose oxidation, showing the outstanding activity arises due to the
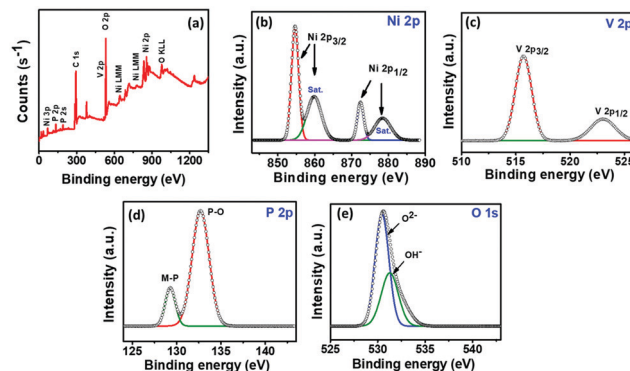

Fig. 4 (a) XP survey spectra and (b–e) XP spectra of the corresponding elements of NiVP/Pi after glucose oxidation.

formation of amorphous nickel vanadium oxyhydroxide/phosphide/phosphate on the electrode surface. This was further supported by stable SEM images and XRD pattern (Fig. S13A, ESI†). Also, the EDS spectra and dot mapping clearly indicated the formation of more oxides (Fig. S13B, ESI†) (post analysis). These results clearly demonstrate the formation of NiV oxide-hydroxide/phosphate/phosphide that then actively participate in enhancing electrochemical glucose oxidation.

4. Conclusion

In summary, we developed a NiVP/Pi-based non-enzymatic electrochemical sensor for glucose sensing, wherein fine tuning the metal ratios could overcome the OER interference. The proposed sensor demonstrated good selectivity among various interferents and an ultrahigh sensitivity of 6.04 mA μM^{-1} cm^{-2} and 4.46 mA μM^{-1} cm^{-2}, with an LOD of 3.7 nM. Additionally, the material exhibited excellent performance in both media (pH 13, pH 7.4), as well with blood serum, demonstrating its great practical applicability.

Conflicts of interest

There are no conflicts to declare.

Acknowledgements

References

1 L. M. T. Phan, T. A. T. Vo, T. X. Hoang, S. P. Selvam, H. L. Pham, J. Y. Kim and S. Cho, *Adv. Mater. Technol.*, 2021, 2100020.

2 J. Van Der Linden, J. B. Welsh, I. B. Hirsch and S. K. Garg, *Diabetes Technol. Ther.*, 2021, **23**, S-1–S-7.

8404 | *J. Mater. Chem. B*, 2021, **9**, 8399–8405

This journal is © The Royal Society of Chemistry 2021

3 P. Katulanda, H. A. Dissanayake, I. Ranathunga, V. Ratnasamy, P. S. Wijewickrama, N. Yogendranathan, K. K. Gamage, N. L. de Silva, M. Sumanatilleke and N. P. Somasundaram, *Diabetologia*, 2020, **63**, 1440–1452.

4 M. Tadic, C. Cuspidi and C. Sala, *J. Clin. Hypertens.*, 2020, **22**, 943–948.

5 O. Kelahmetoglu, M. F. Camlı, A. Kirazoglu, Y. Erbayat, S. Asgarzade, U. Durgun, T. Mehdizade, A. Yeniocak, K. Yildiz and S. Sonmez Ergun, *Int. Wound J.*, 2020, **17**, 1424–1427.

6 J. Wang, *Chem. Rev.*, 2008, **108**, 814–825.

7 A. Bastaki, *Int. J. Diabetes Metab.*, 2005, **13**, 111.

8 P. Balasubramanian, M. Annalakshmi, S.-M. Chen and T.-W. Chen, *Sens. Actuators, B*, 2019, **299**, 126974.

9 A. K. Mishra, D. K. Jarwal, B. Mukherjee, A. Kumar, S. Ratan, M. R. Tripathy and S. Jit, *Sci. Rep.*, 2020, **10**, 1–10.

10 C. Chen, D. Xiong, M. Gu, C. Lu, F.-Y. Yi and X. Ma, *ACS Appl. Mater. Interfaces*, 2020, **12**, 35365–35374.

11 H. Zou, D. Tian, C. Lv, S. Wu, G. Lu, Y. Guo, Y. Liu, Y. Yu and K. Ding, *J. Mater. Chem. B*, 2020, **8**, 1008–1016.

12 D. R. Thévenot, K. Toth, R. A. Durst and G. S. Wilson, *Biosens. Bioelectron.*, 2001, **16**, 121–131.

13 S. Sedaghat, C. R. Piepenburg, A. Zareei, Z. Qi, S. Peana, H. Wang and R. Rahimi, *ACS Appl. Nano Mater.*, 2020, **3**, 5260–5270.

14 E.-H. Yoo and S.-Y. Lee, *Sensors*, 2010, **10**, 4558–4576.

15 S. P. Nichols, A. Koh, W. L. Storm, J. H. Shin and M. H. Schoenfisch, *Chem. Rev.*, 2013, **113**, 2528–2549.

16 M. Waqas, L. Wu, H. Tang, C. Liu, Y. Fan, Z. Jiang, X. Wang, J. Zhong and W. Chen, *ACS Appl. Nano Mater.*, 2020, **3**, 4788–4798.

17 M.-m. Guo, X.-l. Yin, C.-h. Zhou, Y. Xia, W. Huang and Z. Li, *Electrochim. Acta*, 2014, **142**, 351–358.

18 K. Tian, M. Prestgard and A. Tiwari, *Mater. Sci. Eng., C*, 2014, **41**, 100–118.

19 H. Mei, W. Wu, B. Yu, H. Wu, S. Wang and Q. Xia, *Sens. Actuators, B*, 2016, **223**, 68–75.

20 X. Liu, Q. Hu, Q. Wu, W. Zhang, Z. Fang and Q. Xie, *Colloids Surf., B*, 2009, **74**, 154–158.

21 S. Moolayadukkam, S. Thomas, R. C. Sahoo, C. H. Lee, S. U. Lee and H. R. Matte, *ACS Appl. Mater. Interfaces*, 2020, **12**, 6193–6204.

22 G. Gumilar, Y. V. Kaneti, J. Henzie, S. Chatterjee, J. Na, B. Yuliarto, N. Nugraha, A. Patah, A. Bhaumik and Y. Yamauchi, *Chem. Sci.*, 2020, **11**, 3644–3655.

23 M. Yuan, X. Guo, N. Li, Q. Li, S. Wang, C.-S. Liu and H. Pang, *Sens. Actuators, B*, 2019, **297**, 126809.

24 P. Geng, S. Zheng, H. Tang, R. Zhu, L. Zhang, S. Cao, H. Xue and H. Pang, *Adv. Energy Mater.*, 2018, **8**, 1703259.

25 T. Reier, M. Oezaslan and P. Strasser, *ACS Catal.*, 2012, **2**, 1765–1772.

26 N. Padmanathan, H. Shao and K. M. Razeeb, *ACS Appl. Mater. Interfaces*, 2018, **10**, 8599–8610.

27 L.-A. Stern, L. Feng, F. Song and X. Hu, *Energy Environ. Sci.*, 2015, **8**, 2347–2351.

28 Q. Zhang, T. Li, J. Liang, N. Wang, X. Kong, J. Wang, H. Qian, Y. Zhou, F. Liu and C. Wei, *J. Mater. Chem. A*, 2018, **6**, 7509–7516.

29 B. Yao, J. Zhang, T. Kou, Y. Song, T. Liu and Y. Li, *Adv. Sci.*, 2017, **4**, 1700107.

30 A. Dutta, S. Mutyala, A. K. Samantara, S. Bera, B. K. Jena and N. Pradhan, *ACS Energy Lett.*, 2017, **3**, 141–148.

31 H. Lei, M. Chen, Z. Liang, C. Liu, W. Zhang and R. Cao, *Catal. Sci. Technol.*, 2018, **8**, 2289–2293.

32 H. W. Park, J. S. Chae, S.-M. Park, K.-B. Kim and K. C. Roh, *Met. Mater. Int.*, 2013, **19**, 887–894.

33 K. Fan, H. Chen, Y. Ji, H. Huang, P. M. Claesson, Q. Daniel, B. Philippe, H. Rensmo, F. Li and Y. Luo, *Nat. Commun.*, 2016, **7**, 11981.

34 S. Bag, A. Baksi, S. H. Nandam, D. Wang, X. Ye, J. Ghosh, T. Pradeep and H. Hahn, *ACS Nano*, 2020, **14**, 5543–5552.

35 L.-M. Lu, L. Zhang, F.-L. Qu, H.-X. Lu, X.-B. Zhang, Z.-S. Wu, S.-Y. Huan, Q.-A. Wang, G.-L. Shen and R.-Q. Yu, *Biosens. Bioelectron.*, 2009, **25**, 218–223.

36 X. Zhu, Y. Ju, J. Chen, D. Liu and H. Liu, *ACS Sens.*, 2018, **3**, 1135–1141.

37 X. Zhu, S. Yuan, Y. Ju, J. Yang, C. Zhao and H. Liu, *Anal. Chem.*, 2019, **91**, 10764–10771.

38 M. Adeel, M. M. Rahman, I. Caligiuri, V. Canzonieri, F. Rizzolio and S. Daniele, *Biosens. Bioelectron.*, 2020, 112331.

This journal is © The Royal Society of Chemistry 2021

J. Mater. Chem. B, 2021, **9**, 8399–8405 | **8405**